# Determination of Photoinduced Radical Generation Quantum Efficiencies by Combining Chemical Actinometry and 19 F NMR Spectroscopy

Jean Rouillon, Caroline Arnoux, Cyrille Monnereau

# Determination of photoinduced radical generation quantum efficiencies by combining chemical actinometry and $^{19}F$ NMR spectroscopy

Jean Rouillon, Caroline Arnoux and Cyrille Monnereau

Univ. Lyon, ENS Lyon, CNRS, Université Lyon 1, Laboratoire de Chimie, UMR 5182, 46 Allée d'Italie, 69364 Lyon, France.

**ABSTRACT:** We introduce a general and relatively straightforward protocol aimed at determining the absolute photoinduced radical generation efficiency via NMR monitoring. This approach relies on the use of a radical scavenger probe that combines a nitroxide moiety that specifically reacts with radicals, and a trifluoromethyl group used as a $^{19}F$ NMR signaling unit. Using a LED source, which fluence is precisely determined by a chemical actinometry procedure also described herein, the method is used to determine the radical photogeneration quantum yields of three well-known polymerization initiators: Azobisisobutyronitrile (AIBN), 4,4'-Bis(N,N-diethylamino)benzophenone (BDEBP, a derivative of Michler's ethyl ketone) and 2,4,6-trimethylbenzoyl diphenylphosphine oxide (MAPO). The overall good agreement with values previously reported in the literature proves the robustness of this new method. We then extended the study to the precise measurement of the quantum yield of free-radical photogeneration of a newly synthesized photoinitiator used for two-photon direct laser writing. This paper highlights the potential of this methodology for the quantitative determination of photoinduced radical generation efficiency used in many fields of applications.

## INTRODUCTION

Due to the high reactivity of radicals, the quantification of the efficiency their generation proves to be a real challenge in modern photochemistry, particularly in photopolymerization. Thus, while the determination of conversion kinetics has been widely studied described in the literature using various techniques, providing relevant information on radical propagation and termination, photoinduced radical generation stage has been somewhat overlooked in comparison.

This measurement is nonetheless of primary interest to gain understanding about photopolymerization dynamics and consequently optimize photopolymerization efficiency, which initiation largely depends on the quantum efficiency of radical generation. Determination of this parameter is therefore key not only for improving photoinitiator formulation, but also, in combination with above-mentioned techniques more specifically aiming at quantifying radical propagation and termination[1–6] for understanding the mechanisms driving photoinduced polymerization, and therefore controlling the properties of the fabricated structures. This is particularly relevant in the framework of additive fabrication by photopolymerization, as these parameters largely determine such important features as the fabrication threshold, the accessible resolution and the robustness of the fabricated structure.

As mentioned before, photopolymerization, whether it relies on single or multi-photon absorption, requires the use of a photoinitiator (PI) possibly combined with a co-initiator to initiate the reaction.[7] The reactivity of a PI is basically linked to two main physical parameters: i) the ability to interact with light, *i.e.* to absorb one or more photons to undergo a transition from the ground state to the excited state; and then ii) the initiation efficiency which corresponds to the probability for the excited state to generate free radicals that will interact with monomers.[8–10]

The first parameter is relatively easy to evaluate: in the case of conventional UV monophotonic photoinitiators used in most 3D printers, a conventional UV-visible spectrum can be used to obtain the molar extinction coefficient; for non-linear polymerisations, two-photon absorption cross-section can be estimated by Z-scan measurement[10,11] or two-photon excitation fluorescence microscopy[12] for instance.

By comparison, quantification of the radical generation efficiency is by far less straightforward. It often involves indirect methodologies such as Laser Flash Photolysis (LFP)[13,14] studies or EPR spectroscopy of spin-trapped radicals.[6,14] Alternatively, quantification of photogenerated radical after reaction with hydroxyl radicals by potentiometry[15] or High-Performance Liquid Chromatography (HPLC)[16] have also been proposed. However, although interesting as a mean to identify the nature of the generated radical and their kinetics of build-up and consumption, these methodologies suffer from various limitations (complexity of the protocols and availability of the equipment, limitation in the scope of studied radicals…), and alternative methodologies that combine straightforwardness and broad range of use would clearly benefit the field. In this context, luminescence study protocols relying on the use of a radical scavenger nitroxide derivative coupled with a fluorescent moiety have been proposed as powerful and versatile analytical tools: as soon as the nitroxide moiety couples with a radical, intramolecular photoinduced electron transfer luminescence quenching

mechanism is suppressed and the resulting fluorescence increase can be used to track the kinetics of radical build-up.[17–19] However, this approach suffers from the general limitation of fluorescence spectroscopy: it is limited to low concentrations of radical species and can suffer from possible interference if the PI itself displays absorbance or fluorescence in regions overlapping with that of the scavenger.

NMR spectroscopy is a technique of choice to quantitatively investigate product formation over a large range of concentration, and is nowadays routinely available in most molecular and material chemistry laboratories. Nevertheless, NMR is generally not well adapted to radical studies because of their generally short lifetime and most importantly due to their paramagnetic nature that causes the signals to broaden and weaken.[20] Recent attempts to quantify photoinitiations efficiency using NMR spectroscopy have been reported,[21] yet those methodology required initial labeling of the studied PI with $^{13}C$ isotopes.

In this study, we synthesize a nitroxide (2,2,6,6-tetramethylpiperidin-1-yl)oxyl **(**TEMPO) based scavenger, which we functionalize with a trifluoroacetate moiety. We show that, in spite of the paramagnetism of the resulting stable radical molecule, it is still possible to identify a characteristic $^{19}F$ NMR signal, and to track the changes in its chemical shift resulting from combination of the TEMPO to the generated radicals. Due to the high gyromagnetic ratio and natural abundance of $^{19}F$, both the TEMPO scavenger and reaction products are associated with an intense, unique singlet signal, resulting in simple and unambiguous NMR spectra.

Determination of a photochemical quantum efficiency requires an accurate knowledge of the incident photon flux, which is difficult to assess precisely because commercially available power meters are not always reliable.[22] Thus, using 2-nitrobenzaldehyde (NBA) as a chemical actinometer (CA),[23–25] we accurately determine the fluence of the incident light source, and test the robustness of the methodology on a range of different conditions of absorbance and concentrations.

With these data in hand, we monitor the kinetics of radicals photogeneration by $^{19}F$ NMR following of TEMPO scavenger consumption, using various commercial PIs as radical sources, namely azobisisobutyronitrile (AIBN), 4,4'-Bis(*N,N*-diethylamino)benzophenone (Michler's ethyl ketone or BDEBP) and 2,4,6-trimethylbenzoyl diphenylphosphine oxide (MAPO). For all studied systems, measured quantum efficiencies are in good accordance with data reported in the literature, demonstrating the viability of the proposed protocol. As an applicative example, we complete this study by very precisely evaluating the quantum efficiency of a PI synthesized in our laboratory.

## MATERIALS AND METHODS

### General information

All reagents and solvents were used as purchased from commercial suppliers. Synthesis of VShape was depicted by Arnoux *et al.*[26] High-resolution mass spectrometry measurements and elemental analysis were performed at the CRMPO (Centre régional de mesures physiques de l'Ouest, Université de Rennes 1, France).

### NMR analysis

$^{19}F$ NMR spectra were recorded at room temperature on Bruker Avance spectrometers operating at 282 MHz. Dichloromethane-d2 (d, 99.8%) was purchased from Euroisotop. All experiments were carried out on quartz NMR tube equipped with Young's valve (Wilmad 528-LPV-7QTZ). Before each experiment, 0.5 ml of freshly prepared solutions of the compounds to test were systematically degassed with five consecutive freeze-pump-thaw cycles. The accuracy of NMR integration in the titration conditions was checked by comparison of the integration obtained on a test sample acquired with a relaxation time T1 corresponding to that used in standard titration experiments (1 s), T1 being acquired with *ca* five times longer relaxation delays. Measured integration remained unchanged.

### HPLC analysis

HPLC analysis were performed on an Agilent HPLC 1260 apparatus, equipped with ZORBAX Eclipse XDB-C8 reverse phase column. The mobile phase consisted in a 1:1, v/v mixture of acetonitrile and water, with a constant flow rate of 0.5 mL/min. HPLC solvents were purchased from Carlo Erba reagents (HPLC quality) and water was buffered with trifluoroacetic acid (0.5%, v). HPLC chromatograms were obtained with UV detection at 254 nm.

### Irradiation experiments

Excitation spectra were performed on a Horiba Jobin-Yvon Fluorolog-3 spectrofluorimeter. A calibrated integrative sphere (2π steradians covered with spectralon®, model G8 from GMP) was used as described in the literature.[27] A density filter (f = 0.5%) was used to avoid photodamage of the detector. A 365 nm Thorlabs LED (M365L2) equipped with a convex lens (plano-convex f = 25.4 mm, Thorlabs) was chosen as light source, and was set-up close to the irradiated cuvette or sphere so that it was possible to neglect loss of photons along the path. The distance between the LED and the irradiated vessels was kept constant for each experiment (*ca* 10 cm) and the power supply of the LED was tuned with an ammeter (*vide infra*).

| Power | I (mA) |
|---|---|
| Low | 37 |
| Medium | 91 |
| High | 520 |

**Table 1**: Current intensity of the LED power supply chosen for the different experiments

*General procedure A: irradiation of NBA in cuvette*

A stock solution of NBA in acetonitrile was prepared at specific concentrations with volumetric vessels. 2 mL of the solution was transferred into the spectroscopic cuvette with a magnetic stirrer and capped. Irradiation was started with constant stirring. At precise interval of time, 10 µL aliquots of the solution were collected in HPLC amber vials and diluted with 50 µL of acetonitrile.

*General procedure B: irradiation of NBA in NMR tube in integrating sphere*

A stock solution of NBA in acetonitrile was prepared at specific concentration with volumetric vessels. 0.5 mL of the solution was transferred to the NMR tube and irradiation was started. At precise intervals of time, 5 µL aliquots of the solution were collected in HPLC amber vials and diluted in 50 µL of acetonitrile.

**Chemical actinometry**

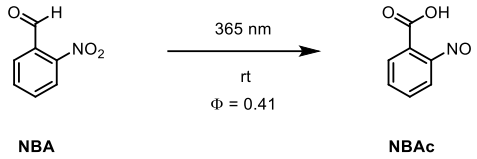


**Scheme 1**: Photoconversion of NBA to NBAc

NBA was used as a chemical actinometer. A conversion quantum yield of 0.41 was considered in the calculations.[28]

The LED power was systematically determined according to general procedures A and B.

Knowing the profile of concentration of NBA as a function of time, we determined the kinetic constant $k_{act}$ of each reaction using a zero order fitting. The validity of the equations used for fluence calculation has already been discussed in the literature[29] as well as the commonly admitted quantum yield of NBA decomposition.[28]

Photon flux $I_0$ of the light source was calculated with the equation (1):

$$I_0 = \frac{k_{act}.N_A.V_c}{\Phi_{NBA}} \quad (1)$$

where $k_{act}$ is the kinetic constant of decomposition (mol.L$^{-1}$.s$^{-1}$) , $N_A$, the Avogadro constant ($N_A$= 6.022.10$^{23}$mol$^{-1}$), $V_c$, the volume of solution (L), $\Phi_{NBA}$, the quantum yield of conversion ($\Phi_{NBA}$ = 0.41) and $I_0$, the photon flux (s$^{-1}$).

Within an integrating sphere, a solution in a NMR tube is not absorbing all the photon flux of the source (the beam width is larger than that of the NMR tube) and effective photon flux $I_{eff}$ then becomes:

$$I_{eff} = \frac{k_{act}.N_A.V_t}{\Phi_{NBA}\left(1 - \frac{L_c}{L_a}\right)} \quad (2)$$

With $L_c$ and $L_a$, the integrated excitation spectra of the sphere (i.e. measured signal of the light source) with and without the sample respectively, $k_{act}$, the kinetic constant (mol.L$^{-1}$.s$^{-1}$) for linear fitting and $V_t$ volume of solution in the tube (L).

The photon flux can be converted to a lamp radiant power P (W) with the equation (3):

$$P = \frac{I_0.h.c}{\lambda} \quad (3)$$

Where, λ is the wavelength of the light source (m), h, the Planck's constant (h = 6.63 × 10$^{-34}$ J.s) and c, the speed of light in vacuum (c = 3.0 x 10$^8$ m.s$^{-1}$).

**Irradiation of cuvette *vs* NMR tube in integrating sphere**

Irradiation in cuvette and in tube were compared using concentrated solutions of NBA (Figure S1 and Tables S1 and S2) for three different LED powers. At such concentrations, absorption of the incident light flux can be considered total in the cuvette (Beer Lambert law indicates a theoretical absorbance A = 15), and can be easily determined in NMR tube by comparing $L_c$ and $L_a$ spectra (*vide supra*). Irradiation experiments in NMR tubes containing highly absorbing solution (*i.e.* strong opacity) at low power give a too slow kinetic, which is not presented. This low power setting was therefore only used for low absorbing solution (*i.e.* A < 1) in the following studies to avoid erratic values. Measurements on concentrated, strongly absorbing solutions in NMR tubes were thus performed using medium or high LED power exclusively. Estimations of the uncertainty U (see equation 4) were made by calculating the relative measurement deviations between the power P, as calculated by the classical actinometry method and the power calculated in a NMR tube $P_{tube}$ (Table S2). The use of an integrating sphere for the irradiation of an NMR tube gives a satisfactory match with the results obtained in a stirred cuvette as shown by the low discrepancies: only 3.1% with the medium power and 1.5% with the high power.

$$U = \frac{P_{tube} - P}{P} \quad (4)$$

**Synthesis of the new probe TEMPO-CF$_3$**

In a dry vessel, trifluoroacetic anhydride (2.0 mL, 14.5 mmol) was added to a solution of TEMPOL (0.5 g, 2.9 mmol) with pyridine (1.6 mL, 20.3 mmol) in dry DCM (20 mL) at 0°C and the mixture was allowed to react for one hour. Reaction mixture was warmed up to room temperature and solvents were removed under vacuum. Crude product was purified by $SiO_2$ column chromatography (PE only to PE:DCM, 1:1 (v/v) to pure DCM) to give TEMPO-CF$_3$ (0.474 g, 58%) as orange powder. $^{19}$F NMR (282 MHz, $CD_2Cl_2$) δ -77.93. HRMS (ESI), calcd for at 269.1233 found 269.1234 (δ = 0 ppm); Elemental analysis calcd for $C_{11}H_{17}NO_3F_3$: C, 49.25, H, 6.39, N, 5.22 found C, 49.09, H, 6.53, N, 5.05.

**NMR evolution of TEMPO-CF$_3$**

*General procedure of irradiation of PI in NMR tube in integrating sphere*

Stock solutions in $CD_2Cl_2$ of PIs and TEMPO-CF$_3$ were prepared at specific concentrations (Table S3) with volumetric vessels. Solutions (0.5 mL in each case) were transferred into the NMR tube. Irradiation was started at t = 0, $^{19}$F NMR spectra were recorded at precise intervals of irradiation time, and the conversion was calculated on the basis of the respective integrations of reactant and product(s).

Ratios of PIs and trapping probe are:

[AIBN] : [TEMPO-CF$_3$] = 1.7:1

[MAPO] : [TEMPO-CF$_3$] = 0.27 : 1

[BDEBP] : [TEMPO-CF$_3$] = 2:1

[V-shape] : [TEMPO-CF$_3$] = 2:1

In all these cases, where a significant excess of PI was used, kinetic constants were calculated by a linear fitting considering a zero order reaction and used in the equation (5) for the determination of the initiation efficiency ($\phi_t$):[29]

$$\Phi_t = \frac{k_t.N_A.V_t}{I_{eff}} \quad (5)$$

where $k_t$ is the kinetic constant of reaction (mol.L$^{-1}$.s$^{-1}$).

For MAPO, where a default amount of PI was used in the determination of $\Phi_t$, concentration of the scavenger over time was plotted with an exponential fitting, considering a first

order reaction and the constant $k_t$ was extrapolated at zero time, with the slope of the tangent line.

## RESULTS AND DISCUSSION

As mentioned above, a key prerequisite in the investigations on photochemical processes consists in precisely assessing the quantity of photons consumed during the reaction. NBA was chosen as a chemical actinometer to quantify the effective fluence of the LED used as an affordable and reliable light source in the experiment described above. The classical approach consists in irradiating a solution of CA in spectroscopic cuvette under constant stirring to monitor the conversion of NBA over time (Scheme 2A).

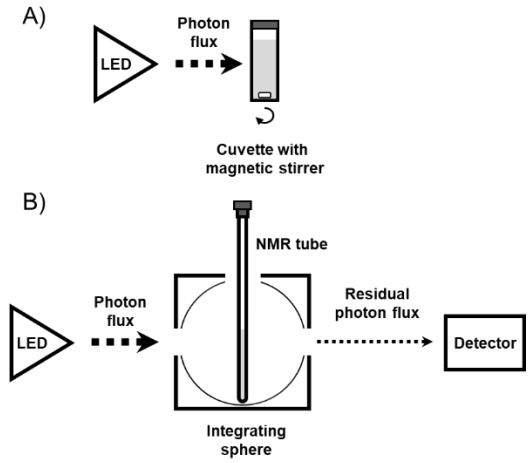


**Scheme 2**: A) Classical approach of photochemical experiment in spectroscopic cuvette with mixing. B) Proposed setup for irradiation of NMR tube in an integrating sphere without mixing

As a beneficial alternative in the framework of this study, we propose the use of an integrating sphere as an optical device to adapt the methodology to the controlled irradiation of an inerted quartz tube, enabling to track the kinetic of reaction by NMR (Scheme 2B). Integrating spheres have been widely used in the literature for accurately determining the optical power of lighting devices[30,31] or the absolute fluorescence quantum yield of molecules at the solid state or in solution.[27] Using this device, the amount of photons actually absorbed by the CA placed in the integrating sphere can be easily evaluated by comparing the transmitted photon flux in the presence and in the absence of the studied sample. The use of an NMR tube as a vessel for the photochemical reaction may be limitative as, in contrast with the cuvette-based measurement, reaction media is not submitted to constant stirring during irradiation. Thus, the accuracy of the method was checked by comparing in-time conversion efficiency of a highly absorbing solution of CA in NMR tube to that measured in a cuvette equipped with magnetic stirring. Same quantum efficiency of conversion of NBA was calculated in NMR tube (in integrating sphere without agitation) and cuvette (with stirring) (Figure S1 and Table S2), which validates the robustness of the protocol.

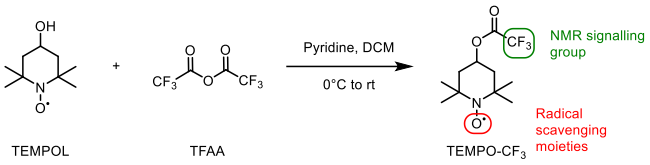


**Scheme 3**: Synthesis of TEMPO-$CF_3$

With this protocol in hand allowing us to accurately determine the power of the incident light source and the absorbance of the tested sample, we next focused on determining radical initiation quantum yields for a series of radical polymerization photoinitiators.

To this end, a new trapping agent was elaborated in order to determine the quantum efficiency of a PI with $^{19}F$ NMR (Scheme 3). Briefly, the one-step synthesis consisted in the reaction between 4-hydroxy-2,2,6,6-tetramethylpiperidin-1-oxyl (TEMPOL) and trifluoroacetic anhydride (TFAA) under basic condition to yield TEMPO-$CF_3$. While the presence of aminoxyl radicals in TEMPO-$CF_3$ induced a marked broadening and spreading-out of the $^1H$ NMR spectrum, making it unexploitable, $^{19}F$ NMR shows up a well resolved, though very slightly broadened, singlet at -77.93 ppm, (Figure 1A), in the expected range of trifluoromethyl chemical shift. Irradiation at appropriate wavelength of a PI in solution induces its dissociation and the scavenging of the generated radicals by TEMPO-$CF_3$ which form a spin trapped photo-products characterized by a new $^{19}F$ NMR signal in the same chemical shift region. The number of new peaks is expected to be dependent of the number of radical species formed by the PI. Evolution of NMR signals, and comparison of the reactant and products peaks integration could be directly used to estimate the initiation efficiency through the measurement of the conversion of TEMPO-$CF_3$ (Figure 1B).

The whole kinetics process at the origin of radical reaction with the scavenger can be conveniently summed up in a two-step model: (i) the radical photogeneration step consists in the absorption of a photon by a PI molecule which undergoes a ground-to-excited state electronic transition. The latter evolves directly or through additional relaxation or inter-system crossing step to the scission of an homolytic bound in the case of Norrish type I PI or a hydrogen atom transfer reaction in the case of Norrish II PI. This first step results in the formation of a radical $PI^{\cdot}$ that will (ii) react with the scavenger TEMPO-$CF_3$ ($T^{\cdot}$) to form the spin trapped photo-product (S). The whole process is somewhat reminescent of the initiation step in radical polymerization (except that $PI^{\cdot}$ addition does not take place on a vinyl monomer but on a radical scavenger), and therefore the quantum efficiency determined using this protocol can be more accurately approximated to the initiation quantum efficiency than to the radical generation quantum efficiency *per se*.

| | **Norrish 1** | **Norrish 2** |
|---|---|---|
| First step | $PI + h\nu \xrightarrow{k_1} PI_1^{\cdot} + PI_2^{\cdot}$ | $PI + R\text{-}H \xrightarrow{k_1} R^{\cdot} + PIH^{\cdot}$ |
| Second step | $\begin{cases} PI_1^{\cdot} + T^{\cdot} \xrightarrow{k_2} S \\ PI_2^{\cdot} + T^{\cdot} \xrightarrow{k_2'} S \end{cases}$ | $\begin{cases} R^{\cdot} + T^{\cdot} \xrightarrow{k_2} S \\ PIH^{\cdot} + T^{\cdot} \xrightarrow{k_2'} S \end{cases}$ |

**Table 2**: Different mechanisms of reaction between PI and TEMPO-$CF_3$

We postulate that the fraction of initiator PI that is converted to radicals $PI^{\cdot}$ react directly with $T^{\cdot}$ to form S with a high kinetic rate of *ca* $10^7$-$10^9$ $mol^{-1}.s^{-1}$ typical of radical recombination reactions.[17,19] According to the steady-state approximation, considering $k_1 << k_2$, the photogeneration of radicals is the rate determining step of the whole process. Thus, the rate of conversion of $T^{\cdot}$ is considered equal to the product of the formation rate of radical $PI^{\cdot}$ by the so called "initiator efficiency factor" f (equation (6)):

$$-\frac{d[T^{\cdot}]}{dt} = \frac{d[PI^{\cdot}]}{dt} f \quad (6)$$

This factor (0 < f < 1) is an empirical parameter aimed at taking into account side reactions of primary radical recombination that may limit the availability of a generated radical to be involved in a chain reaction initiation event. The evolution of the concentration of TEMPO-$CF_3$ over time is fitted with a linear (pseudo zero order, in the case where PI is present in large excess relative to the scavenger) or exponential function (when PI is the limiting reactant). Initiation efficiency (Φ) is defined as the ratio of photons generating "efficient" radicals (*i.e.* radicals involved in an initiation step) on photons absorbed by the solution, and obtained with the equation (5).

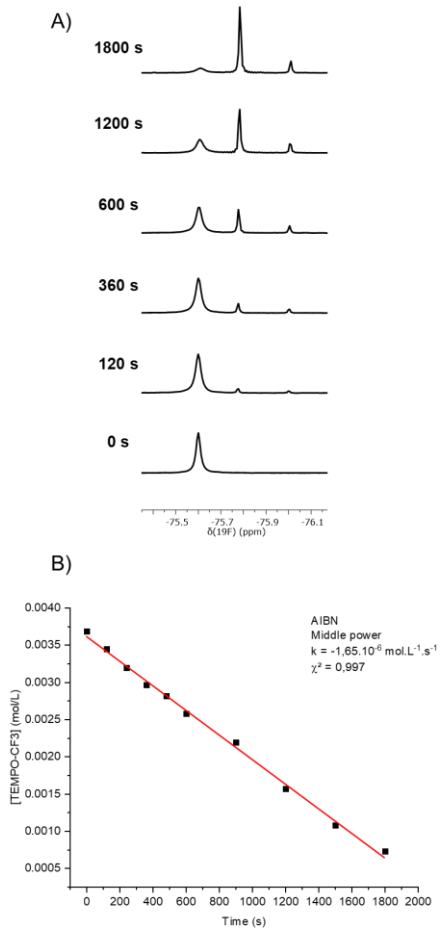


**Figure 1**: A) Series of $^{19}$F-NMR spectra of TEMPO-$CF_3$ with AIBN under 365 nm irradiation in $CD_2Cl_2$; B) Plots of [TEMPO-$CF_3$] time (the black squares represent the experimental concentrations and the red line, the exponential decay fitting the data)

An example of the kinetic of irradiation of AIBN in presence of TEMPO-$CF_3$, in deuterated dichloromethane ($CD_2Cl_2$) solution, is presented on the figure 1B. Concentration of TEMPO-$CF_3$ was determined over time with $^{19}$F NMR. In these conditions, zero order fitting of the concentration decay *versus* irradiation time yields a kinetic constant of k = $1.65.10^{-6}$ $mol.L^{-1}.s^{-1}$ which, knowing the incident light power of P = 2.48 mW, affords an efficient initiation quantum efficiency of 0.22 for AIBN. Considering the strong influence of the solvent on the recombination process of butyronitrile radical and thus on the *f* parameter, this value is in a relatively good agreement with the previous value of 0.40[32] determined in acetonitrile.

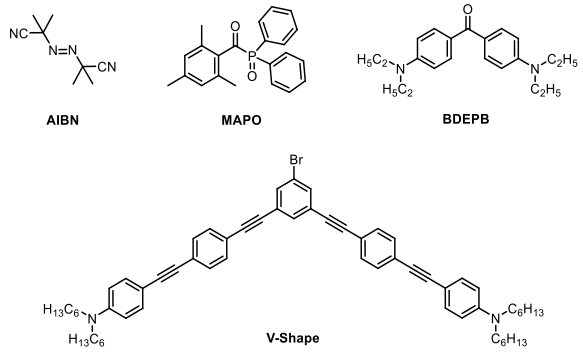


**Scheme 4**: Chemical structures of the studied PIs

| | AIBN | MAPO | BDEBP | Vshape |
|---|---|---|---|---|
| Φ | 0.22 | 1.21 | 0.0043 | 0.00049 |

**Table 3**: Photochemical quantum efficiency of the studied PIs

Photoinitiation efficiency of MAPO, another Norrish I initiator classically used in photopolymerization[33] was also evaluated (Figure S2). In this case, initial attempts to work with similar concentrations as those used with AIBN resulted in erratic and irreproducible QY values, largely exceeding unity. In order to circumvent this issue, MAPO was introduced in a lower concentration, with an excess of scavenger ([MAPO]: [TEMPO-$CF_3$] = 0.27 : 1). Fitting, in this case, the conversion profile to an exponential trade (first order model, consistent with the limiting amount of MAPO in the mixture), and measuring the initial rate by considering the tangent at the origin of the resulting curve, we obtained a photoinitiation quantum yield of $\Phi_i$=1.22, allowing to determine (assuming f=1, consistent with the high addition efficiency of acylphosphine oxide radicals photoproducts)[34] a photodissociation quantum yield of $\Phi_{diss}$ = 0.61, which here again turned out in good agreement with previously published values: 0.55[35] and 0.7[36] in acetonitrile and 0.5 to 0.6[37] in dichloromethane.

BDEBP is an archetypical Norrish II initiator, known as a strong absorber PI with comparatively lower radical generation efficiency, as it involves a bimolecular reaction as initiation step, and ideally requires a co-initiator. The quantum efficiency of BDEBP was estimated at $4.30.10^{-3}$ (Figure S3),

which is consistent with values found in literature (for Michler's ketone in the absence of co-initiator: 0.03[38]).

V-Shape, which structure is specifically designed to promote large two-photon absorption cross-section, [26] showed unsurprisingly an even lower initiation quantum efficiency of $4.9.10^{-4}$ (Figure S4). This value explains in retrospect why, in spite of a much increased two-photon absorption cross-section measured at 532 nm (1500 GM vs 77 GM for BDEBP), two-photon polymerization threshold is only lowered by a factor *ca* 5.

## CONCLUSIONS

By combining i/ a precise chemical actinometric protocol, ii/ the use of an integrating sphere giving accurate access to the ratio of incident light absorption and iii/ a new TEMPO-based radical scavenger featuring a trifluoroacetate moiety, we show that it is possible to evaluate the quantum efficiency of photoinduced initiation step of different Norrish I and Norrish II type PIs using a straightforward $^{19}F$ NMR protocol. This protocol is herein applied to series of commercial PIs of different nature (Norrish I and Norrish II types), either commercially available or synthetized in our laboratory: calculated quantum yields for the commercial PIs are generally consistent with values found in literature. In the case of the synthesized PI, this study provides a rational explanation to results previously obtained in a recently published work, in particular the difference in polymerization energy threshold between BDEBP and V-Shape. To illustrate the versatility of the as depicted protocol, it is worth mentioning that it could be successfully applied in this study to PIs with radical generation efficiency ranging from 1.2 to below $5\ 10^{-4}$. We believe that the methodology proposed in this paper could constitute an interesting benchmark for systematic comparisons of newly synthesized PIs *vs* commercially available or previously synthesized ones. In addition to radical photoinitiation processes, we would also like to point out that the adaptation of a chemical actinometry protocol to measurements in an NMR tube as proposed and validated in this paper is easily applicable to the investigation on the quantum yields of other photoinduced events such as photocatalyzed chemical synthesis, photoisomerization or photocyclisation processes, which are topics that we are currently investigating.[39,40]

## ASSOCIATED CONTENT

### Supporting Information

Detailed data about chemical actinometry measurements on spectroscopic cuvette vs. integrating sphere (Figure S1 and Tables S1-S2); Kinetics of others PIs with their respective $^{19}F$ NMR series (Figures S2-S4 and Table S3).

The Supporting Information is available free of charge on the ACS Publications website.

## AUTHOR INFORMATION


### Corresponding Author

**Cyrille Monnereau** – Université Lyon, ENS Lyon, CNRS, Université Lyon 1, Laboratoire de Chimie, UMR 5182, 69364 Lyon, France ; orcid.org/0000-0002-8928-2416 ;
Email : cyrille.monnereau@ens-lyon.fr

### Authors

**Jean Rouillon** – Université Lyon, ENS Lyon, CNRS, Université Lyon 1, Laboratoire de Chimie, UMR 5182, 69364 Lyon, France ; orcid.org/0000-0001-7823-7575 ;

**Caroline Arnoux** – Université Lyon, ENS Lyon, CNRS, Université Lyon 1, Laboratoire de Chimie, UMR 5182, 69364 Lyon, France ; orcid.org/0000-0002-6984-8099 ;



### Funding Sources

C.A. thanks the Agence Nationale de la Recherche ANR for financial support (PhD grant) in the framework of the "New3DPrint" project (ANR-17-CE08-0037).


### Notes

The authors declare no competing financial interest.


## ACKNOWLEDGMENT

All authors would like to thank Dr. Frédéric Chaput for the special design of the homemade holder for the integrating sphere. Dr. Akos Banyasz and Sandrine Denis-Quanquin are warmly thank for stimulating discussions regarding chemical actinometry and NMR quantification.


## REFERENCES


(1) Buback, M.; Gilbert, R. G.; Hutchinson, R. A.; Klumperman, B.; Kuchta, F.-D.; Manders, B. G.; O'Driscoll, K. F.; Russell, G. T.; Schweer, J. Critically Evaluated Rate Coefficients for Free-Radical Polymerization, 1. Propagation Rate Coefficient for Styrene. *Macromolecular Chemistry and Physics* **1995**, *196* (10), 3267–3280. https://doi.org/10.1002/macp.1995.021961016.

(2) Beuermann, S.; Buback, M. Rate Coefficients of Free-Radical Polymerization Deduced from Pulsed Laser Experiments. *Progress in Polymer Science* **2002**, *27* (2), 191–254. https://doi.org/10.1016/S0079-6700(01)00049-1.

(3) Buback, M.; Egorov, M.; Junkers, T.; Panchenko, E. Termination Kinetics of Dibutyl Itaconate Free-Radical Polymerization Studied via the SP–PLP–ESR Technique. *Macromolecular Chemistry and Physics* **2005**, *206* (3), 333–341. https://doi.org/10.1002/macp.200400358.

(4) Buback, M. Propagation Kinetics in Radical Polymerization Studied via Pulsed Laser Techniques. *Macromolecular Symposia* **2009**, *275–276* (1), 90–101. https://doi.org/10.1002/masy.200950111.

(5) Buback, M.; Schroeder, H.; Kattner, H. Detailed Kinetic and Mechanistic Insight into Radical Polymerization by Spectroscopic Techniques. *Macromolecules* **2016**, *49* (9), 3193–3213. https://doi.org/10.1021/acs.macromol.5b02660.

(6) Krys, P.; Matyjaszewski, K. Kinetics of Atom Transfer Radical Polymerization. *European Polymer Journal* **2017**, *89*, 482–523. https://doi.org/10.1016/j.eurpolymj.2017.02.034.

(7) Andrzejewska, E. Photopolymerization Kinetics of Multifunctional Monomers. *Progress in Polymer Science* **2001**, *26* (4), 605–665. https://doi.org/10.1016/S0079-6700(01)00004-1.

(8) Efficiency of a Photopolymerization Reaction. In *Photoinitiators for Polymer Synthesis*; John Wiley & Sons, Ltd, 2012; pp 103–122. https://doi.org/10.1002/9783527648245.ch7.

(9) Photosensitive Systems. In *Photoinitiators for Polymer Synthesis*; John Wiley & Sons, Ltd, 2012; pp 73–88. https://doi.org/10.1002/9783527648245.ch5.

(10) Zhou, R.; Malval, J.-P.; Jin, M.; Spangenberg, A.; Pan, H.; Wan, D.; Morlet-Savary, F.; Knopf, S. A Two-Photon Active Chevron-Shaped Type I Photoinitiator Designed for 3D Stereolithography. *Chem. Commun.* **2019**, *55* (44), 6233–6236. https://doi.org/10.1039/C9CC02923K.

(11) Ajami, A.; Husinsky, W.; Liska, R.; Pucher, N. Two-Photon Absorption Cross Section Measurements of Various Two-Photon Initiators for Ultrashort Laser Radiation Applying the Z-Scan Technique. *J. Opt. Soc. Am. B, JOSAB* **2010**, *27* (11), 2290–2297. https://doi.org/10.1364/JOSAB.27.002290.

(12) Mettra, B.; Liao, Y. Y.; Gallavardin, T.; Armagnat, C.; Pitrat, D.; Baldeck, P.; Bahers, T. L.; Monnereau, C.; Andraud, C. A Combined Theoretical and Experimental Investigation on the Influence of the Bromine Substitution Pattern on the Photophysics of Conjugated Organic Chromophores. *Phys. Chem. Chem. Phys.* **2018**, *20* (5), 3768–3783. https://doi.org/10.1039/C7CP06535C.

(13) Hola, E.; Ortyl, J.; Jankowska, M.; Pilch, M.; Galek, M.; Morlet-Savary, F.; Graff, B.; Dietlin, C.; Lalevée, J. New Bimolecular Photoinitiating Systems Based on Terphenyl Derivatives as Highly Efficient Photosensitizers for 3D Printing Application. *Polym. Chem.* **2020**, *11* (4), 922–935. https://doi.org/10.1039/C9PY01551E.

(14) Reactivity of Radicals toward Oxygen, Hydrogen Donors, Monomers, and Additives: Understanding and Discussion. In *Photoinitiators for Polymer Synthesis*; John Wiley & Sons, Ltd, 2012; pp 399–454. https://doi.org/10.1002/9783527648245.ch18.

(15) Brainina, K. Z.; Gerasimova, E. L.; Kasaikina, O. T.; Ivanova, A. V. Antioxidant Activity Evaluation Assay Based on Peroxide Radicals Generation and Potentiometric Measurement. *Analytical Letters* **2011**, *44* (8), 1405–1415. https://doi.org/10.1080/00032719.2010.512687.

(16) Sun, L.; Bolton, J. R. Determination of the Quantum Yield for the Photochemical Generation of Hydroxyl Radicals in TiO2 Suspensions. *J. Phys. Chem.* **1996**, *100* (10), 4127–4134. https://doi.org/10.1021/jp9505800.

(17) Moad, G.; Shipp, D. A.; Smith, T. A.; Solomon, D. H. Measurements of Primary Radical Concentrations Generated by Pulsed Laser Photolysis Using Fluorescence Detection. *J. Phys. Chem. A* **1999**, *103* (33), 6580–6586. https://doi.org/10.1021/jp990892t.

(18) Coenjarts, C.; García, O.; Llauger, L.; Palfreyman, J.; Vinette, A. L.; Scaiano, J. C. Mapping Photogenerated Radicals in Thin Polymer Films: Fluorescence Imaging Using a Prefluorescent Radical Probe. *J. Am. Chem. Soc.* **2003**, *125* (3), 620–621. https://doi.org/10.1021/ja028835s.

(19) Blinco, J. P.; Fairfull-Smith, K. E.; Morrow, B. J.; Bottle, S. E. Profluorescent Nitroxides as Sensitive Probes of Oxidative Change and Free Radical Reactions†. *Aust. J. Chem.* **2011**, *64* (4), 373–389. https://doi.org/10.1071/CH10442.

(20) Bertini, I.; Luchinat, C.; Parigi, G.; Pierattelli, R. NMR Spectroscopy of Paramagnetic Metalloproteins. *ChemBioChem* **2005**, *6* (9), 1536–1549. https://doi.org/10.1002/cbic.200500124.

(21) Ruhland, K.; Habibollahi, F.; Horny, R. Quantification and Elucidation of the UV-light Triggered Initiation Kinetics of TPO and BAPO in Liquid Acrylate Monomer. *Journal of Applied Polymer Science* **2020**, *137* (6), 48357.

(22) Kuhn, H. J.; Braslavsky, S. E.; Schmidt, R. Chemical Actinometry (IUPAC Technical Report). *Pure and Applied Chemistry* **2004**, *76* (12), 2105–2146. https://doi.org/10.1351/pac200476122105.

(23) Allen, J. M.; Allen, S. K.; Baertschi, S. W. 2-Nitrobenzaldehyde: A Convenient UV-A and UV-B Chemical Actinometer for Drug Photostability Testing. *Journal of Pharmaceutical and Biomedical Analysis* **2000**, *24* (2), 167–178. https://doi.org/10.1016/S0731-7085(00)00423-4.

(24) Willett, K. L.; Hites, R. A. Chemical Actinometry: Using o-Nitrobenzaldehyde to Measure Lamp Intensity in Photochemical Experiments. *J. Chem. Educ.* **2000**, *77* (7), 900. https://doi.org/10.1021/ed077p900.

(25) Galbavy, E. S.; Ram, K.; Anastasio, C. 2-Nitrobenzaldehyde as a Chemical Actinometer for Solution and Ice Photochemistry. *Journal of Photochemistry and Photobiology A: Chemistry* **2010**, *209* (2), 186–192. https://doi.org/10.1016/j.jphotochem.2009.11.013.

(26) Arnoux, C.; Konishi, T.; Van Elslande, E.; Poutougnigni, E.-A.; Mulatier, J.-C.; Khrouz, L.; Bucher, C.; Dumont, E.; Kamada, K.; Andraud, C.; Baldeck, P.; Banyasz, A.; Monnereau, C. Polymerization Photoinitiators with Near-Resonance Enhanced Two-Photon Absorption Cross-Section: Toward High-Resolution Photoresist with Improved Sensitivity. *Macromolecules* **2020**. https://doi.org/10.1021/acs.macromol.0c01518.

(27) Porrès, L.; Holland, A.; Pålsson, L.-O.; Monkman, A. P.; Kemp, C.; Beeby, A. Absolute Measurements of Photoluminescence Quantum Yields of Solutions Using an Integrating Sphere. *J Fluoresc* **2006**, *16* (2), 267–273. https://doi.org/10.1007/s10895-005-0054-8.

(28) Galbavy, E. S.; Ram, K.; Anastasio, C. 2-Nitrobenzaldehyde as a Chemical Actinometer for Solution and Ice Photochemistry. *Journal of Photochemistry and Photobiology A: Chemistry* **2010**, *209* (2–3), 186–192. https://doi.org/10.1016/j.jphotochem.2009.11.013.

(29) Stadler, E.; Eibel, A.; Fast, D.; Freißmuth, H.; Holly, C.; Wiech, M.; Moszner, N.; Gescheidt, G. A Versatile Method for the Determination of Photochemical Quantum Yields *via* Online UV-Vis Spectroscopy. *Photochemical & Photobiological Sciences* **2018**, *17* (5), 660–669. https://doi.org/10.1039/C7PP00401J.

(30) Envall, J.; Kärhä, P.; Ikonen, E. Measurements of Fibre Optic Power Using Photodiodes with and without an Integrating Sphere. *Metrologia* **2004**, *41* (4), 353–358. https://doi.org/10.1088/0026-1394/41/4/018.

(31) Carrasco-Sanz, A.; Martín-López, S.; Corredera, P.; González-Herráez, M.; Hernanz, M. L. High-Power and High-Accuracy Integrating Sphere Radiometer: Design, Characterization, and Calibration. *Appl. Opt., AO* **2006**, *45* (3), 511–518. https://doi.org/10.1364/AO.45.000511.

(32) Alvarez, J.; Encinas, M. V.; Lissi, E. A. Solvent Effects on the Rate of Polymerization of 2-Hydroxyethyl Methacrylate Photoinitiated with Aliphatic Azo Compounds. *Macromolecular Chemistry and Physics* **1999**, *200* (10), 2411–2415. https://doi.org/10.1002/(SICI)1521-3935(19991001)200:10<2411::AID-MACP2411>3.0.CO;2-G.

(33) Sun, H.-B.; Kawata, S. Two-Photon Photopolymerization and 3D Lithographic Microfabrication. In *NMR • 3D Analysis • Photopolymerization*; Fatkullin, N., Ikehara, T., Jinnai, H., Kawata, S., Kimmich, R., Nishi, T., Nishikawa, Y., Sun, H.-B., Eds.; Apvances in Polymer Science; Springer: Berlin, Heidelberg, 2004; pp 169–273. https://doi.org/10.1007/b94405.

(34) Arsu, N.; Reetz, I.; Yagci, Y.; Mishra, M. K. *Photoinitiated Radical Vinyl Polymerization*; CRC Press Taylor & Francis Group: New York, 2009; Vol. 8.

(35) Ganster, B.; Fischer, U. K.; Moszner, N.; Liska, R. New Photocleavable Structures. Diacylgermane-Based Photoinitiators for Visible Light Curing. *Macromolecules* **2008**, *41* (7), 2394–2400. https://doi.org/10.1021/ma702418q.

(36) Allonas, X.; Lalevée, J.; Fouassier, J.-P. Investigation of Cleavage Processes in Photoinitiators: From Experiments to Molecular Modeling. *Journal of Photochemistry and Photobiology A: Chemistry* **2003**, *159* (2), 127–133. https://doi.org/10.1016/S1010-6030(03)00177-1.

(37) Sumiyoshi, T.; Schnabel, W.; Henne, A.; Lechtken, P. On the Photolysis of Acylphosphine Oxides: 1. Laser Flash Photolysis Studies with 2,4,6-Trimethylbenzoyldiphenylphosphine Oxide. *Polymer* **1985**, *26* (1), 141–146. https://doi.org/10.1016/0032-3861(85)90069-2.
(38) Suppan, P. Solvent and Temperature Effects in the Photoreduction of Ketones. *Berichte der Bunsengesellschaft für physikalische Chemie* **1968**, *72* (2), 321–326. https://doi.org/10.1002/bbpc.19680720258.
(39) Ghiazza, C.; Debrauwer, V.; Monnereau, C.; Khrouz, L.; Médebielle, M.; Billard, T.; Tlili, A. Visible-Light-Mediated Metal-Free Synthesis of Trifluoromethylselenolated Arenes. *Angewandte Chemie International Edition* **2018**, *57* (36), 11781–11785. https://doi.org/10.1002/anie.201806165.
(40) Adouama, C.; Keyrouz, R.; Pilet, G.; Monnereau, C.; Gueyrard, D.; Noël, T.; Médebielle, M. Access to Cyclic Gem-Difluoroacyl Scaffolds via Electrochemical and Visible Light Photocatalytic Radical Tandem Cyclization of Heteroaryl Chlorodifluoromethyl Ketones. *Chem. Commun.* **2017**, *53* (41), 5653–5656. https://doi.org/10.1039/C7CC02979A.